Heliyon 8 (2022) e10529

Contents lists available at ScienceDirect

Heliyon

journal homepage: www.cell.com/heliyon

Research article

Effects of yttrium doping on structural, electrical and optical properties of barium titanate ceramics

Suravi Islam [a,*], Nazia Khatun [a], Md. Shehan Habib [a], Syed Farid Uddin Farhad [a], Nazmul Islam Tanvir [a], Md. Aftab Ali Shaikh [c,d], Samia Tabassum [d], Dipa Islam [d], Md. Sajjad Hossain [d], Ayesha Siddika [d]

[a] Industrial Physics Division, BCSIR Laboratories, Dhaka, Bangladesh Council of Scientific and Industrial Research (BCSIR), Dhaka 1205, Bangladesh
[c] Department of Chemistry, University of Dhaka, Dhaka 1000, Bangladesh
[d] Bangladesh Council of Scientific and Industrial Research (BCSIR), Dhaka 1205, Bangladesh

ARTICLE INFO

Keywords:
Barium titanate
X-ray diffraction
Dielectric properties
Scanning electron microscopy
Optical properties

ABSTRACT

In this report, we study the Yttrium-doped Barium Titanate (Y-BT) $Ba_{1-x}Y_xTiO_3$ (with x = 0.00, 0.01, 0.03, 0.05, 0.07 mmol) perovskite ceramics synthesized by sol-gel method. The as-made powder samples were pressed into a pellet shape and subsequently sintered at 1300 °C for 5 h in air. The structural, morphological, electrical, and optical properties of the synthesized samples were investigated by X-ray diffraction (XRD), field emission scanning electron microscopy (FESEM), impedance analyzer, and UV-Vis-NIR Spectroscopy respectively. The XRD study revealed the formations of single phase tetragonal structure of Barium Titanate (BT) with ~23–33 nm mean crystallite size. The crystallite size increases initially with Y-doping, found at about 33 nm for x = 0.01, and reduces for increase in Y^{3+} concentration further. The microstructural study from FESEM depicts the uniform distribution of compact and well-faceted grain growth for Y-BT in contrast with undoped barium titanate. The average grain size (~0.29–0.78 μm) of the Y-BT decreases with increasing doping concentration. Frequency-dependent impedance analyses show enhanced dielectric properties like dielectric constant, quality factor, and conductivity with low dielectric loss in the presence of Yttrium. The optical bandgap energy (~2.63–3.72 eV) estimated from UV-Vis-NIR diffuse reflection data shows an increasing trend with a higher concentration of yttrium doping.

1. Introduction

Barium titanate ($BaTiO_3$, BT) is a common ferroelectric material, extensively used in the electrical and electronic industries due to its many excellent and useful features such as high dielectric permittivity, positive temperature coefficient of resistivity (PTCR), high-voltage tunability, ferroelectricity, pyroelectricity and piezoelectricity [1, 2, 3]. Perovskite materials derived from BT have many applications, including positive temperature coefficient devices, pulse generating devices, infrared detectors, voltage tunable devices in microwave electronics, multilayer ceramic capacitors (MLCCs), piezoelectric and ultrasonic actuators, thermal sensors and controllers, and microwave devices for piezoelectric transducers and charge storage devices [4, 5, 6] and so forth.

The structure of barium titanate is based on the ABO_3 general formula and comprises perovskite-based metal oxide minerals that crystallize at room temperature with a stable tetragonal structure [7, 8, 9]. Recent research has focused on substituting Ba^{2+} or Ti^{4+} with alternative ions of equal ionic sizes to control the grain size [8] and to improve the ferroelectric and dielectric characteristics of BT [10, 11].

An effective way to improve the electrical properties of the ceramic materials is impurity doping, where metal doping is commonly used [1, 12] even though the properties of the doping metal are yet to be understood [13]. Rare earth elements such as Ho^{3+}, Er^{3+}, Yb^{3+}, Sm^{3+}, Dy^{3+}, and Y^{3+} doped BT are the most imperative and widely used dopants for fabricating the MLCCs applications [12, 13]. Among them, Y_2O_3 is usually worked as a dopant in the industrial fabrication of MLCCs because it shows similar properties and is less expensive [14]. Y^{3+} doping improves the insulation resistance, results in high conductivity and permittivity, inhibits the growth of dielectric grains, dielectric loss and high leakage current used in manufacturing MLCCs [15]. It also enhances

* Corresponding author.;
E-mail addresses: suravii@yahoo.com, suraviislambcsir@gmail.com (S. Islam).

https://doi.org/10.1016/j.heliyon.2022.e10529
Received 8 May 2022; Received in revised form 18 July 2022; Accepted 31 August 2022

the temperature stability of BT, changes the lattice parameters, shifts the Curie temperature, and reduces the sinterability of BT as Y_2O_3 conserve a high melting point [16].

The ionic radius of Y^{3+} (0.9 Å, 1.234 Å for CN = 6,12) is in-between that of Ba^{2+}(1.61 Å) and Ti^{4+} (0.605 Å). Therefore, Y^{3+} might replace either the Ba^{2+} or Ti^{4+}cation site in the BT lattice, which helps enhancing the lifetime of the MLCCs. However, the dielectric characteristics of BT also rely on doping type, preparation method, microstructure, Ba:Ti ratio, dopant amount, solubility, and electrical properties of dopant [15]. Zhi et al. [17] showed solubility of Y^{3+}at the A site of BT while sintered in air at 1440–1470 °C. P. Ren et al. [18]observed enhanced conductivity in BT by supplementing Y^{3+} at the Ba-site, that is linked to electron compensation. The impacts of yttrium doping in the structural, electrical, and optical properties of BT ceramics have been explored where the doping raised the dielectric constant, grain size, modified curie temperature, and reduced band gap energy of BT [18, 19, 20]. Jianquan Qi *et al.* [12] observed that Y-BT becomes a semiconductor when the sintering temperature is near 1250 °C. A theoretical study of Y-BT by A. Alshoaibi *et al.* [15] showed that the dielectric constants were increased due to the introduction of Yttrium.

Many synthesis approaches have been reported, for instance, conventional solid-state reaction, hydrothermal technique, and co-precipitation methods for fabricating barium titanate used for electrical device applications [2, 9, 10, 11, 12, 13]. However, to the best of our knowledge, sol-gel is an excellent tool for fabricating new compositions because of a chance to control the stoichiometry and homogeneity of the achieved material and require lower thermal condition with simple lab equipment [21]. In our research, we attempt to prepare Yttrium doped $BaTiO_3$ by sol-gel method at different doping concentrations and carry out the sintering in air. To understand the role of Y^{3+} addition, we analyze the prepared materials and study the structural, electrical, and optical properties, giving particular attention to the stoichiometric ratio of $BaTiO_3$ and the semiconducting nature of its application in MLCCs.

2. Materials and method

Analytical grade Barium Acetate ($Ba(CH_3COO)_2$; ENSURE, ACS, 99%; Germany), Yttrium oxide (Y_2O_3; Sigma-Aldrich; 99%, China), and Titanium oxide (TiO_2; Sigma-Aldrich; 99%, Germany), Tartaric acid and polyvinyl alcohol (PVA) were taken as starting chemicals. BT and Y-BT ceramic materials were synthesized by sol-gel method following the formula $Ba_{1-x}Y_xTiO_3$. Certain amount of yttrium oxide (x = 0.00, 0.01, 0.03, 0.05 and 0.07 mmol) solution was added to acetic acid (0.2 M) solution with constant stirring at 65–70 °C for 2 h. During heating and stirring, the solution beaker was covered with a watch glass, and a clear solution was observed. After that, Barium acetate $Ba(CH_3COO)_2$ was added to the yttrium solution and stirred smoothly at the same temperature for 2 h. Tartaric acid solution and TiO_2 solution were added to the reaction mixture to get the final solution. Eventually, 10% polyvinyl alcohol (PVA, as an esterification agent) was added in the mixed solution and stirred for 6–8 h at 60–90 °C. The solution gradually became concentrated and formed white monolithic gel.

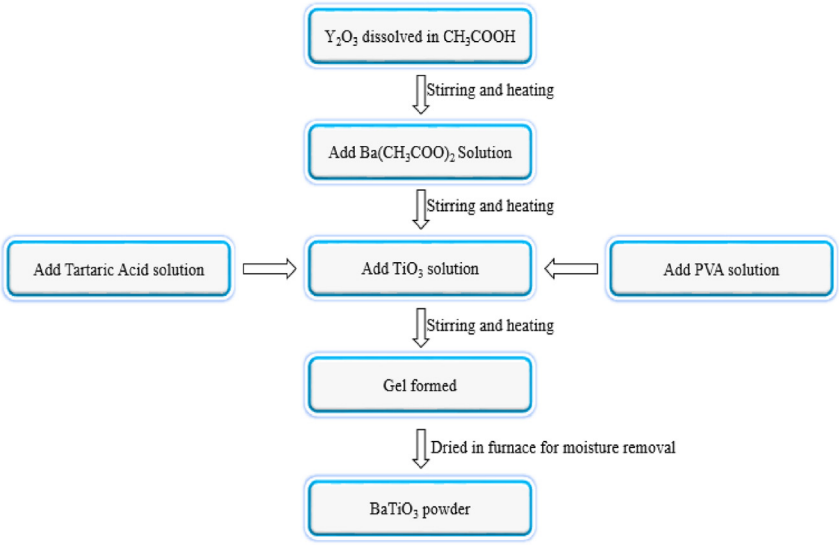

Flow Chart illustration of synthesis method

The gel was further dried in a furnace at 90 °C for moisture removal and pre-sintered at 700 °C for 3 h in air. Subsequently, the samples were ground, for binding aqueous solution of Polyvinyl alcohol (4%) were mixed, and were pressed applying pressure 2 ± 0.5 M Pa for 1 min to form disk-shaped pellets. Finally, the as prepared disks were sintered at 1300 °C for 5 h in a programmable muffle furnace (Nabertherm, Germany) in the air.

After sintering the synthesized samples, all the characterizations were performed at room temperature. The structural and crystallographic properties of the pellets were measured from an X-ray diffractometer (XRD) (EMMA; GBC Scientific Equipment, Australia) by means of Cu_Kα radiation (I = 0.15406 nm) and Raman spectroscopy (MacroRAM, Japan) analysis. The morphology of the pellets was studied by Field Emission Scanning Electron Microscopy (FESEM), JSM-7610F, Japan. For obtaining optical properties, an ultraviolet–visible-near-infrared (UV–Vis-NIR) spectrometer (UV-2600, Shimadzu, Japan) was used having a wavelength from 220 to 1400 nm range. A conductive layer of silver paste (Demetron Leipzegrstr.10, Germany) was coated on the fined surface of the pellets to measure the dielectric properties. The electrical parameters were taken from the Impedance Analyzer (Agilent 4294A, 40 kHz to 120 MHz).

3. Results and discussion

3.1. Structural properties: XRD analysis

X-ray diffraction (XRD) patterns for Yttrium doped Barium Titanate (Y-BT) $Ba_{1-x}Y_xTiO_3$ at different doping concentrations (x = 0.00, 0.01, 0.03, 0.05, and 0.07 mmol) are displayed in Figure 1. The powdered samples exhibit a perovskite structure, as evidenced by the diffraction pattern in the illustration. The observed diffraction peaks are 001, 101,

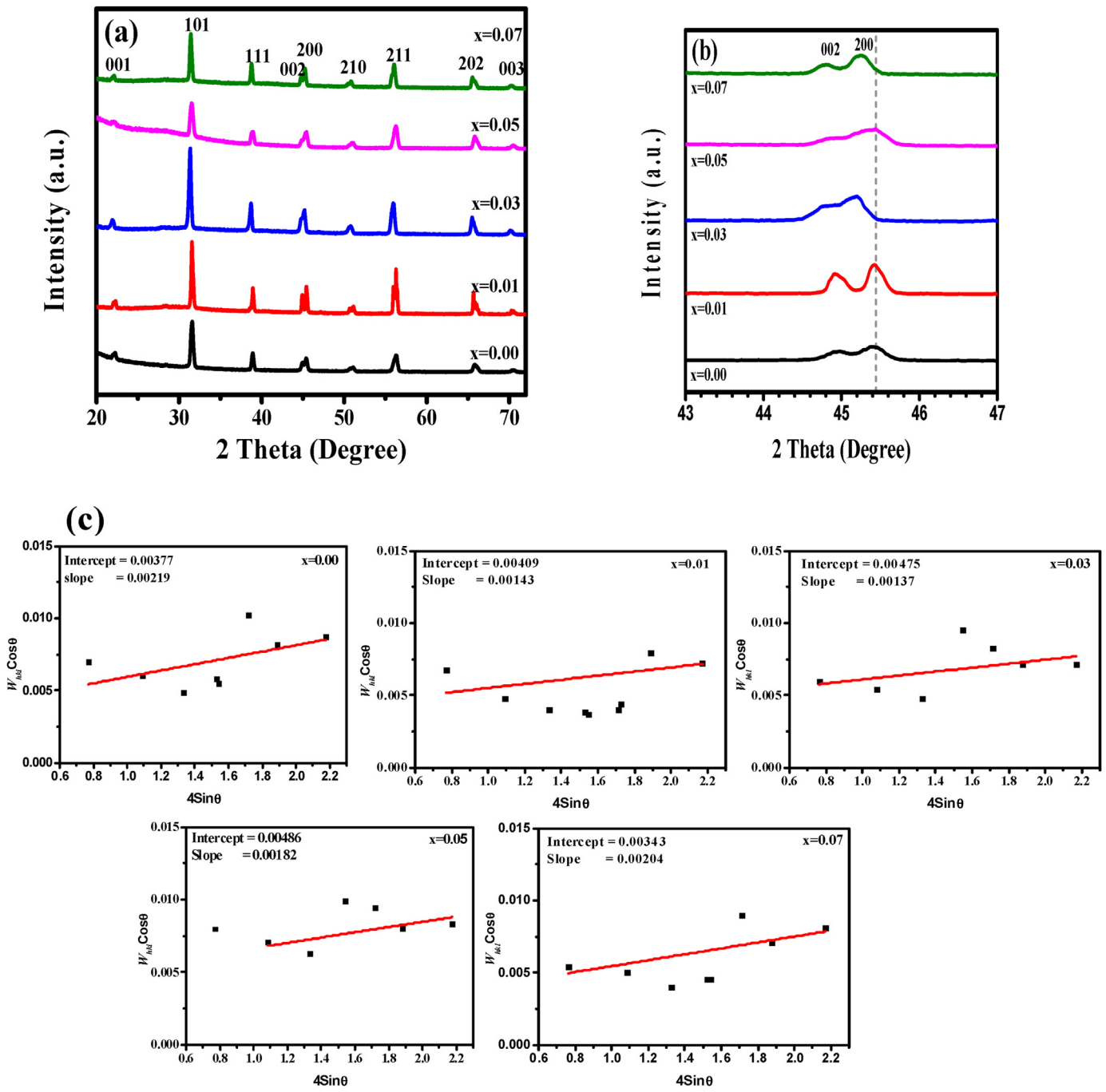

Figure 1. 1(a) X-ray diffraction pattern, 1(b) The peaks associated with the 002, 200 planes at around 45° and 1(c) Williamson and Hall (W–H) analysis of $Ba_{1-x}Y_xTiO_3$ (x = 0.00, 0.01, 0.03, 0.05 and 0.07 mmol) Sintered at 1300 °C.

111, 002, 200, 210 corresponds to 2θ° = 22.22°, 31.42°, 38.78°, 44.96°, 45.42° & 50.82° respectively also matches with literatures [1, 22]. The average diffraction peaks were matched with JCPDS card no. 00-005-0626, indicating a tetragonal formation of $BaTiO_3$ ceramic for all the samples except x = 0.03 which shows pseudocubic structure macroscopically [13]. Yittrium dissolved up to certain depth in the BT particle smoothly which causes the reduction of tetragonality. A similar result was found where Kim. *et al.* reported that the ferroelectricity of BT decreases strongly at grain size below 7 μm, and changes to pseudocubic from tetragonal structure [16]. The phase changes are generally described as a combination of tetragonal and cubic phases and presented as pseudocubic phase. The XRD pattern of BT powder shows a pure tetragonal phase, while it evidences a decrease of the tetragonality with a higher concentration of Y_2O_3 also matches with our results.

The diffractogram showed a double peak at about 2θ ° ≈ 45° illustrated in Figure 1(b) indicating the tetragonal ferroelectric phase with 002, 200 planes. The (002) and (200) peaks reveals a minor distortion and plane shift in the direction of lower angle along with apparent enhancement in lattice parameter. This is ascribed to the enlargement of cell volume of crystals to some extent because of the incorporation of Y^{3+} at Ba^{2+} ions. Structural evaluation can be clearly seen from the characteristics peaks (002, 200) at around 45°.

The lattice parameters of the tetragonal structure were calculated by utilizing (*hkl)* values and inter-planar spacing with the relation.

Table 1. Lattice parameter (a) & (b), lattice parameter (c), tetragonality (c/a), Cell volume, Crystalline size and strain of $Ba_{1-x}Y_xTiO_3$ samples.

Sample $Ba_{1-x}Y_xTiO_3$	Lattice parameter "a = b" (Å)	Lattice parameter "c" (Å)	Tetragonality (c/a)	Cell Volume (Å^3)	Crystalline size, D (nm)		Strain, ε	
					Deby-Shearer	Williamson-Hall method	Deby-Shearer ($\times10^{-3}$)	Williamson-Hall method ($\times10^{-3}$)
x = 0.00	3.9921	4.0274	1.0098	64.184	23	36.8	5.599	2.19
x = 0.01	3.9904	4.0325	1.0106	64.210	33	33.9	4.440	1.43
x = 0.03	4.0081	4.0291	1.0052	64.726	28	29.2	5.052	1.37
x = 0.05	3.9887	4.0376	1.0123	64.237	20	28.61	6.495	1.82
x = 0.07	4.0054	4.0427	1.0093	64.857	28	40.4	4.680	2.04

$$\frac{1}{d^2}=\frac{(h^2+k^2)}{a^2}+\frac{l^2}{c^2} \tag{1}$$

where d denotes inter-planar spacing. The samples' average crystalline size (t) was measured for the intensity 002 and 200 peak using the Debye-Scherrer formula [23].

$$t=\frac{0.9\lambda}{\beta cos\theta} \tag{2}$$

where λ (1.540562Å) is the X-rays wavelength, β is the full width half maximum (FWHM), and θ is the Bragg's diffraction angle. Lattice parameters (a, b, and c), tetragonality (c/a) and Crystalline size were determined by Eqs. (1) and (2) and presented in Table 1.

The crystalline size of BT increases initially for x = 0.01 mmol of Yttrium and then decreases with doping further; for x = 0.07 mmol, the cell volume increases accordingly. Tetragonality or grain lattice parameters can be influenced by the existence of defects and impurities [12] for a high sintering temperature of 1300 °C. It indicates the perovskite phase formation with enhanced crystallinity of Y-BT. The changes of lattice parameters c values indicate the integration of doping metal Y^{3+} in Ba-site. However, the addition of Yittrium in the Titanium site can't be ignored as it is capable of occupying either Ba or Ti site. Enhancement of oxygen vacancy, grain growth, and grain boundary diffusion sometimes predominates on the sintering temperatures and is also susceptible to temperature, impurities, and orientation of the crystal.

The volume of the unit cell was determined by multiplying a^2*c and the measured data were shown in Table 1. By adding Y^{3+}, we were able to greatly enhance the tetragonal matrix of Y-BT, which went from 64.184 Å^3 at (x = 0.0) to 64.857 Å^3 at (x = 0.07). The samples' lattice parameters (a, c) rise when yttrium content increases, leading in an increase in unit cell volume, because the electronic density and ionic radii of Y varies. This type of enlargement has also been observed for zirconium doping in a tetragonal matrix of $BaTiO_3$ [24].

Williamson and Hall (W–H) suggested that lattice-strain in the material initiated by crystallite defect and distortion are the main features responsible for the broadening of diffraction peaks [25].

$$W_{hkl} = W_{crystalite} + W_{strain} \tag{3}$$

Here, W_{hkl} corresponds to the full-width peak at half maxima intensity, correlated to the lattice strain and crystalline sizes according to the W–H method. The broadening ascribed to the lattice strain can be denoted as [26].

$$W_{strain}=4\varepsilon\, tan\theta \tag{4}$$

Rearranging W–H Eq. (3) we get

$$W_{hkl}cos\theta=\frac{0.9\lambda}{C_s}+4\varepsilon\, sin\theta \tag{5}$$

The W–H plots of $W_{hkl}\, cos\theta$ versus 4sinθ for Y-BT samples are illustrated in Figure 1(c). The lattice strain and the average crystalline size, were determined from the slope and the y-intercept of linear line; obtained values according eq. (4, 5) are represented in Table 1. Moreover, both of the Debye-Scherrer and W–H analysis stated that the crystalline size and strain of all the samples followed the same trend [26].

A typical geometrical factor that reflects the durability of the perovskite structure is the tolerance factor. Widespread acceptance has been accorded to Goldschmidt's tolerance factor, t, as an indicator of the development of the perovskite structure. It provides an estimate of the number of voids are favorable for the A site cation. The Goldschmidt's tolerance factor of the synthesized samples were measured following relation [27].

$$\boldsymbol{t}=\frac{(\boldsymbol{r_A}+\boldsymbol{r_o})}{\sqrt{2}(\boldsymbol{r_B}+\boldsymbol{r_O})} \tag{6}$$

where r_A, r_B, and r_O are the ionic radii of the A, B, and O oxygen ions, respectively, of the ABO_3 type perovskite structure in Eq. (6). The tolerance factor for pure BT ceramic, t = 1.06 suggested a deformation of crystal structure where r_A (Ba^{2+}) = 1.61 Å, r_B (Ti^{4+}) = 0.605 Å, and r_O (O^{2-}) = 1.4 Å. The incorporation of Y_2O_3, (r (Y^{3+}) = 0.9 Å) into BT directed to the reduction of the Goldschmidt's tolerance factor. The values of t for $Ba_{1-x}Y_xTiO_3$ samples are calculated and presented in Table 2 values range from 1.061 to 1.052, showing a similar result as ref [9]. Here, it is expected A-site and B-site will be occupied by large ions and small ions respectively and both A and B sites with different partitioning for each ion will be occupied by intermediate ions. However, considering tolerance factors to assess between ions in different sites is simply a qualitative measure [9].

The X-ray density of the synthesized samples have determined by equation [29].

$$\rho_x=\frac{ZM}{N_A a^3} \tag{7}$$

Here, Z, M, N_A and a is the number atoms per unit cell, the molar mass, Avogadro's number and lattice constant of the samples respectively. The bulk density have been calculated by following formula [28].

$$\rho_b=\frac{m}{\pi t r^2} \tag{8}$$

where m, t, and r are mass, thickness, and radius of the prepared pallet samples, respectively. The porosity of synthesized Y-BT samples was estimated by means of the following relation [29].

Table 2. Tolerance factor(t), Bulk density (ρ_b), X-ray density, (ρ_x) and Porosity (P) of $Ba_{1-x}Y_xTiO_3$.

Sample $Ba_{1-x}Y_xTiO_3$	Tolerance factor(t)	Bulk Density, ρ_b (ρ_b (g cm^{-3}))	X-ray density, (ρ_x (g cm^{-3}))	Porosity, P (%)
x = 0.00	1.061	2.490	6.033	58.72
x = 0.01	1.059	2.266	6.018	55.70
x = 0.03	1.054	1.330	5.944	77.62
x = 0.05	1.049	2.748	5.965	53.93
x = 0.07	1.044	1.752	5.883	70.22

$$P = \left(1 - \frac{\rho_b}{\rho_x}\right) \times 100\% \quad (9)$$

ρ_x, ρ_b are the X-ray density and bulk density of the prepared samples and porosity are measured using Eqs. (7), (8), and (9). The thickness of the ($Ba_{1-x}Y_xTiO_3$) pellets were 0.32 cm, 0.38 cm, 0.25 cm, 0.15 cm and 0.27 cm for x = 0.00, x = 0.01, x = 0.03, x = 0.05, x = 0.07 respectively. The calculated values of X-ray density, bulk density and porosity of the Y-BT samples are summarized in Table 2. The X-ray density and bulk density decreases but the increase in porosity occurs with increase in doping concentration.

3.2. Raman spectroscopy

Raman spectroscopy is used to analyze the structure and phase shift of Y-BT ceramics and examine vibrational, rotational and other low-frequency modes [30]. Figure 2 illustrates the Raman spectra of $Ba_{1-x}Y_xTiO_3$ (x = 0.00, 0.01, 0.03, 0.05, 0.07 mmol) were performed from 100 cm^{-1} to 1000 cm^{-1} at room temperature. The characteristic four different peaks (denoted by vertical lines) of tetragonal Y-BT ceramic powder are reported to be arising from the splitting of transverse (TO) and longitudinal (LO) photons [18]. Raman peaks were observed at about 262 cm^{-1} (A_1 (TO)), 307 cm^{-1} (B_1, E (TO + LO)), 512 cm^{-1} (A_1 (TO), E (TO)) and 719 cm^{-1} (A1 (LO), E (LO)) respectively. The detected bands were matched with $BaTiO_3$-based ceramics by ref. [31]. The peaks denoted by A1, B1, and E (TO + LO), TO2, LO2 vibrational modes respectively and reveal the tetragonal symmetry (*P4mm*) of $BaTiO_3$ ferromagnetic state [32] shows similar results to other researchers [30, 33]. When there is sufficient dopant content in BT so that it crosses over the point of phase transition from tetragonal to cubic, the tetragonal phase *(P4mm)* of Raman active modes remains inactive in the perfect cubic phase (*Pm3m*) following the forbidden Raman selection rules. Besides, an intense band of 512 cm^{-1} sustained at the tetragonal phase above Tc. With the increase in Y^{3+}content the band turn into narrow and keen also a vivid change at low frequencies was observed. No significant shift in wavelength was noticed in the spectra of Y-BT but became steeper with an increase in yttrium concentration which indicate enhanced crystallinity for higher Y^{3+}concent that also demonstrate similar consequence with the XRD analysis [34].

3.3. Microstructure analysis

The microstructure of Yttrium doped Barium Titanate, $Ba_{1-x}Y_xTiO_3$ ceramics sintered at 1300 °C for 5 h are presented in Figure 3(a, b, c, d, e). The FESEM micrograph provides the surface morphology of the samples, which illustrates a structure of hexagonal nature, well-faceted grains with distinct and separate boundaries. However, agglomerated dispersion of some grains was also found. The coarse grains are shown in Figure 3(a) were in the process of agglomeration, whereas the boundaries with fine grains gradually became a blur. Figure 3(c') shows the magnified view of c with 1 μm scale bar illustrating the mechanism of formation of layers.

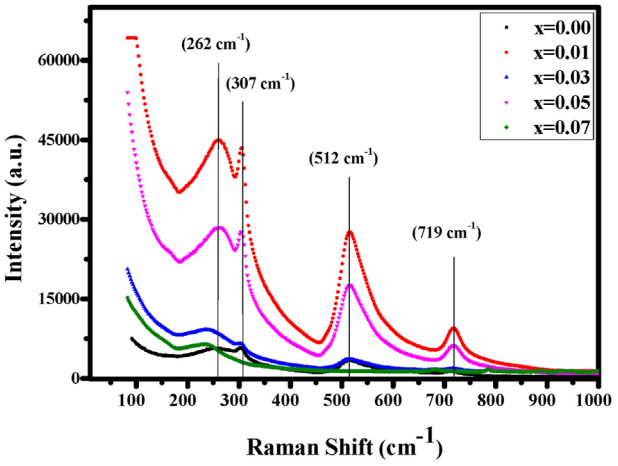

Figure 2. Raman spectra of pure and Yttrium doped barium titanate.

The average grain size of undoped BT (0.28μm) is smaller than that of Y-BT samples, increased with the doping concentration stated in Figure 3(a, b, c, d, e) and Table 3 has close harmony with other researchers [35]. Since agglomeration occurs, the lowest average grain size was found 0.614 μm at x = 0.05. The liquid phase sintering effect, grain boundary diffusion, and defect reaction play an important role in promoting grain growth. It reveals the grain distribution is more uniform, compact, and has a denser structure with less porosity percentage. The highest value of grain size (0.778 μm) was found for x = 0.03 samples, and the porosity is high as well.

3.4. Electrical property

3.4.1. Frequency-dependent electrical properties

The charge-holding ability of a material at a specific frequency often corresponds to its dielectric properties. This is because BT is an extremely effective dielectric that has a promising future in ceramic capacitors [36]. The dielectric constant can be determined using a common capacitive measurement method that is

$$\varepsilon = \frac{Cd}{\varepsilon_0 A} \quad (10)$$

where C, d and A is the capacitance, thickness and the area of the of the BT pellet and ε_0 is the permittivity (8.85 × 10^{-12} F/m) of free space mentioned in Eq. (10).

The variation of dielectric constant (έ) for $Ba_{1-x}Y_xTiO_3$ ceramics are shown in Figure 4(a) in the frequency range 1 kHz–100 kHz. The dielectric constant falls significantly and exhibits a keen drop in the low-frequency range, up to 20 kHz and remains constant at a higher frequency array of 100 kHz. However, high έ was found at the order of 10^3 as a usual trend similar with other researchers [3, 38]. With the exception of x = 0.03, Y-BT has a larger charge-accumulating efficiency than un-doped BT. Furthermore, Figure 4(a) shows that the capacitance exhibits a dramatic decline in the low-frequency band (100–1000 Hz). The capacitive response is suppressed at high frequency when the charge carriers can follow an ac frequency and are more likely to be mobile. At low frequencies, έ is higher and more diffuse because they need more time for ion reversal with varying fields owing to interfacial polarization. This might be related to electrode polarization, in which electric charges follow the applied electric field, whereas it declines to zero at higher frequencies; charges cannot follow the field at high frequencies, resulting in a lower value of έ [37].

The dielectric properties depend on two factors that dominate grain size and the second phase formation during the sintering process. Many researchers have investigated the relationship between particle size, dielectric constant, internal stress, ferroelectric domains, and grain boundary layers [39]. Apart from x = 0.03, all Y-BT samples have a nominal dielectric loss and strong dielectric constant stability. These findings hold a lot of promise for microwave device applications. The dielectric loss appears to increase with the addition of x = 0.03 percent, which might be due to an increase in grain boundary defects brought on by the growth of the Y-BT phase in the material. The largest dielectric loss of any sample is caused by the addition of x = 0.03 percent, demonstrating inadequate insulation resistance reported as ref [3].

The process of energy dissipation is related to the dielectric system's loss tangent (tanδ). Figure 4(b) illustrates the frequency dependence of dielectric loss from 40 kHz–100 kHz and showed lower values for Y-doped BT than un-doped one. Furthermore, tanδ experiences a decreasing trend with increasing frequency and after that, remains stable at a higher frequency of 20 kHz and above for all the samples, except for x = 0.03. These

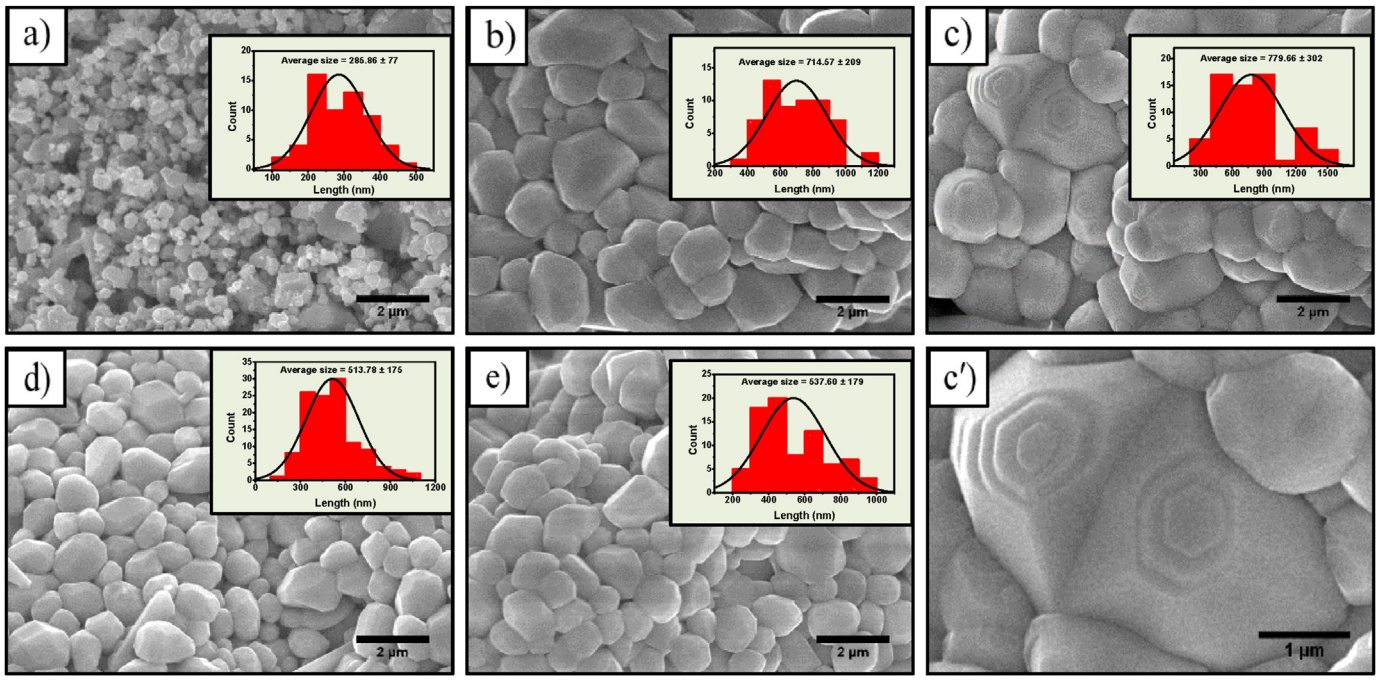

Figure 3. FESEM micrographs with grain size distribution curve of $Ba_{1-x}Y_xTiO_3$ (where a, b, c, d, e are x = 0.00, 0.01, 0.03, 0.05 and 0.07 respectively and c' is magnified view of c).

Table 3. Table of average grain Size, band gap, Transition temperature (T_c), dielectric constant (έ), and dielectric loss (Tanδ) for yttrium doped barium titanate.

Sample $Ba_{1-x}Y_xTiO_3$	Average grain Size (μm)	Band gap (eV)	Transition Temperature (T_c)	Dielectric constant (έ)@ Room temperature (freq, 40 Hz)	Dielectric constant (έ)@ Room temperature (freq, 589 Hz)	Dielectric constant (έ) At transition temperature@ 10 kHz	Tanδ At room temperature (frequency, 40 Hz)
$BaTiO_3$	0.287	2.63	120	–	2179	117	2.77
$Ba_{0.09}Y_{0.01}TiO_3$	0.715	3.12	115	1211	1112	186	0.13
$Ba_{0.07}Y_{0.03}TiO_3$	0.779	3.72	115	639	277	473	0.36
$Ba_{0.05}Y_{0.05}TiO_3$	0.614	3.17	115	2501	2148	807	0.10
$Ba_{0.03}Y_{0.07}TiO_3$	0.638	3.70	115	2180	2109	109	0.15

consequences are in agreement with the fact that Y is usually added with the donor dopants in order to reduce the dissipation factor. The amount of dielectric loss displays dispersion at low frequency, but it continues to decrease and reaches zero for x = 0.0, 0.03.0.07 at high frequency. This is because charges may influence the field orientation at low frequencies owing to a large amount of time, but this diminishes as frequency increases, resulting in a decrease in dielectric loss [37].

The resistivity graph of the synthesized $Ba_{1-x}Y_xTiO_3$ samples are drawn in Figure 5(a), showing the dependence aligned with frequency on the concentration of Y^{3+} at room temperature. The high concentration of Y^{3+} doping results in relatively elevated resistivity compared to undoped BT. In the beginning resistivity ascends with the density of donor and then it decreases, the highest resistivity was obtained for x = 0.01 whereas the lowest for x = 0.00.

Electricity can flow freely through a specimen, which is measured by its electrical conductivity. Figure 5(b) explicitly states that, in general, conductivity is frequency independent up to 10 kHz, but that all samples then suffer a sharp upward trend. As the frequency rises,

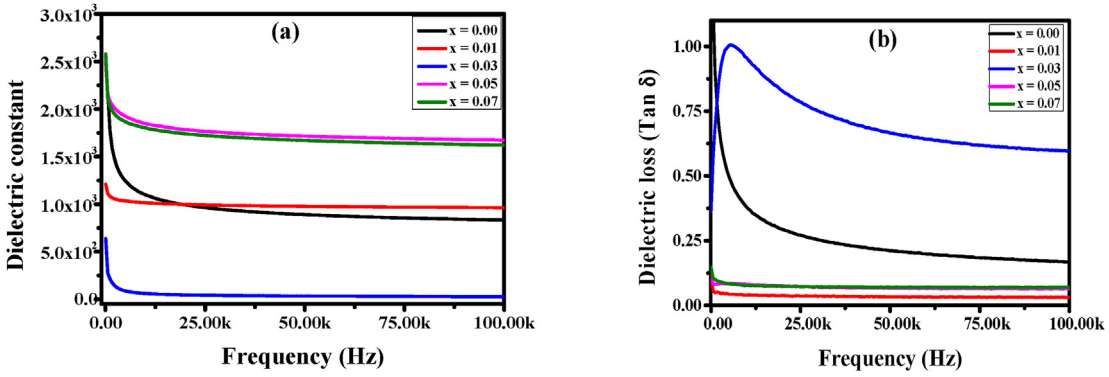

Figure 4. 4(a) Variation of dielectric constant with frequency 4(b)Variation of dielectric loss (tanδ) with frequency for yttrium doped barium Titanate.

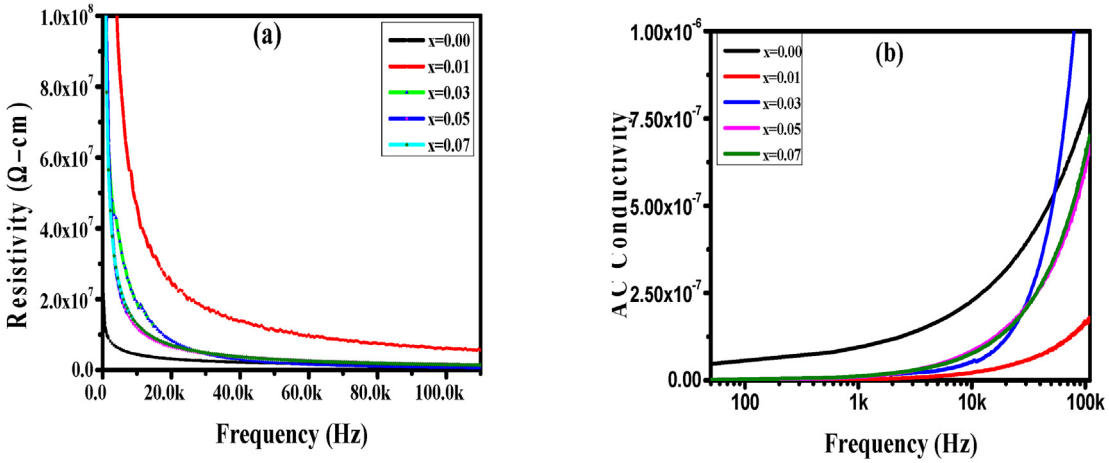

Figure 5. 5(a) Plot of Resistivity vs. frequency and 5(b) AC conductivity vs. frequency.

the likelihood of an electron passing through Y^{3+} ions at grain boundaries rises as well, which leads to more ions exchanging and an increase in conductivity.

3.4.2. Temperature-dependent electrical properties

Figure 6(a) shows the variation of the dielectric constant (έ) of Y-BT as a function of temperature in the frequency region of 10 kHz. Temperature-dependent relative permittivity curve of the samples sintered at 1300 °C for 5 h was measured.

The Y-BT sample exhibits a sharp peak at the Curie temperature, T_c with the value of έ, and then decreased with the increasing frequency (highest 807, for x = 0.05). At room temperature έ is low, but shows higher value up to a specific point at higher temperature, and then drops again at further elevation of temperature. However, at increasing temperatures, dipole mobility rises owing to continuous heat increase, causing huge dipole vibrations, diverting the polarization mechanism, and lowering the dielectric constant value, as predicted according to the Debye model [37].

The characteristics of the capacitance with temperature stability are related to the structure of core-shell and volume of a core shell assumed. In Figure 6, it is apparent that the phase transition temperature of un-doped BT shows a higher value than doped Y-BT. In comparison with the ferroelectric to paraelectric phase, T_c of undoped BT was found at 120 °C, and 115 °C for all increasing concentrations of Y-BT mentioned in Table 3. Moreover, it is noticeable that the dielectric constant increases as content of Y^{3+} rises and reached at maximum for x = 0.05 whereas found 117 for un-doped BT. Similar results were found in ref, albeit the loss tangent exhibits a different tendency to decrease with temperature (Figure 6(b)) similar results were found in ref [38].

3.5. Optical properties

The UV-Visible absorption spectra of un-doped and Y-doped $BaTiO_3$ were displayed in Figure 7(a) in the 200–1200 nm wavelength range. An increase in the absorbance of all the samples from 350 to 550 nm confirms that Y-BT is an absorber in the ultraviolet range. To analyze the electron transition type and band structure, it is very important to measure the dependence of the optical absorption coefficient,α on photon energy. The band gap energy of the materials can be computed using Tauc relationship [39].

$$(\alpha h\nu)^n = A(h\nu - E_g) \tag{11}$$

where A denotes an energy-dependent constant that relies on transition probability, α is the absorption coefficient, hν photon energy, and Eg is the optical band gap in Eq. (11). The nature of the transition is denoted by exponent n; n = 2 for direct and 1/2 for indirect allowed transition, $BaTiO_3$ compound shows the indirect transition.

The absorption spectra were measured by the Kubelka-Munk function from converted diffuse reflectance spectra (DRS) using the following relation [40].

$$F(R_\alpha) = \frac{(1 - R_\alpha)^2}{2R_\alpha} \tag{12}$$

$$[(FR_\alpha)h\nu]^{\frac{1}{n}} = A(h\nu - Eg) \tag{13}$$

where R_α is the diffuse reflectance and Eg is determined considering formula (12, 13) from the extrapolation of the linear part of the Tauc plot

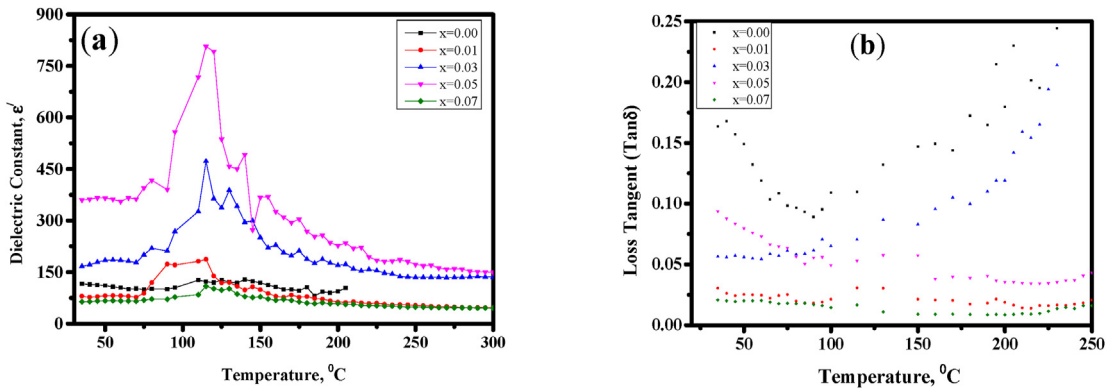

Figure 6. 6(a) Plot of the temperature dependence of the dielectric constant and 6(b) Loss tangent vs. temperature for Y-BT at 10 kHz frequency.

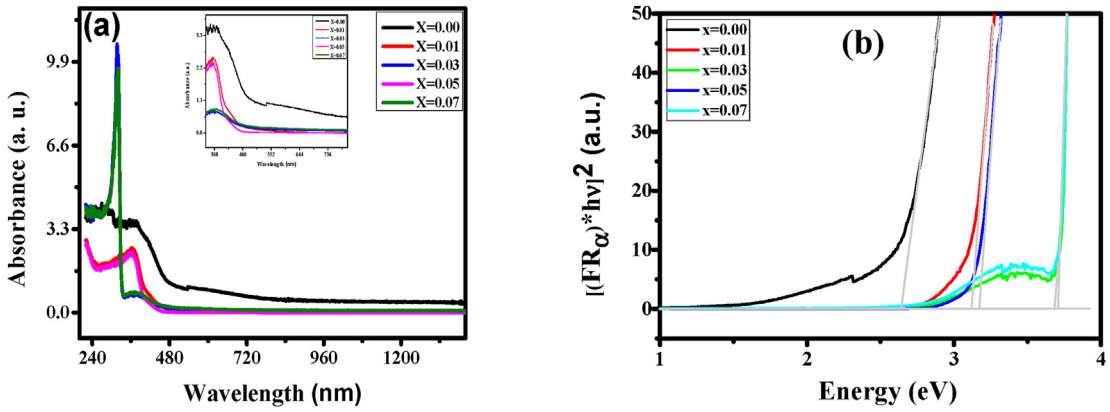

Figure 7. 7(a) UV–Vis absorption spectra 7(b) Bandgap estimation from Tauc plot of Y-BT samples.

up to the intercept of the energy axis.Therefore, by fitting a straight line to the curve of the plot hν vs FR_α a bandgap value, Eg can be obtained in the axis where the quantity must be zero. As estimated from Figure 7(b), the bandgap of x = 0.00–2.63 eV is much lower than those of x = 0.01 and above ~3.12–3.72 eV, suggesting that samples grown with lower concentrations are crystalline in nature, presumably composed of much lower size crystallites compared to x = 0.00 samples.

The primary absorption bands of $Ba_{1-x}Y_xTiO_3$ (x = 0.00, 0.01, 0.03, 0.05, 0.07 mmol) samples were located within the 258–384 nm wavelength range. Here, the maximum absorption wavelength of un-doped BT is 295 nm and has increased further in the presence of Y^{3+} for x = 0.01, 0.03, 0.05, 0.07 mmol, and we found 365 nm, 317 nm, 362 nm, and 320 nm, respectively.

The optical band gap, E_g, is related inversely to the grain size and crystallinity reported by ref. [22] for $BaTiO_3$/ZnO ceramics and ref. [41] for barium titanate nanoparticles. However, Table 3 shows that both the band gap and average grain size increased with doping concentration. On the other hand, Eg increases gradually as the particle size (smaller than 11.5 nm) decreases and this effect may occur due to the micrometer scale of bulk Y-BT materials [41]. These results indicate that the size effect of BaTiO3 can be observed in sizes smaller than 11.5 nm. The shift in Eg values may be caused by a number of factors such as the crystal size, strain carrier density, and existing of slight impurities [42].

Grain size, shape, oxygen vacancy, and defects are some parameters were involved in optical absorption. The region of energy that isolates the valence band and conduction band is the band gap which contains no electronic state at all. The binding energy increased in the presence of Yttrium and the utmost 3.72 eV found for x = 0.03 mmol concentration also corresponds with the report in ref. [41] due to larger particles of $BaTiO_3$ bulk.

4. Conclusions

Yttrium doped Barium titanate Y-BT ceramics were successfully synthesized by sol-gel method. We investigated the impact of Y^{3+} doping on the structural, electrical, and optical properties of $Ba_{1-x}Y_xTiO_3$ sintered at 1300 °C for 5 h in air with x = 0.00, 0.01, 0.03, 0.05, and 0.07 mmol. Tetragonal and pseudo-cubic structures were seen in the structural properties derived from X-ray diffraction, and this was further validated by Raman spectroscopy. The crystallite size increased initially with Y-doping and declined through a further addition in dopant content up to x = 0.05. FESEM micrographs depicted the formation of uniform, compact, and well-faceted grain growth for Y-BT in contrast with BT. An increase in average grain size in doped samples was noticed in comparison with BT ceramics (~0.29–0.78 μm). The optical bandgap energy (~2.63–3.72 eV) calculated from the Tauc plot exhibited an increasing trend with a higher concentration of Y^{3+}. The dielectric measurement demonstrated that materials respond to input temperature and frequency. However, as the concentration of Y^{3+} rises, the Curie temperature falls and stays at 115 °C. Frequency-dependent impedance analyses showed enhanced dielectric properties like dielectric constant, quality factor, and conductivity with low dielectric loss in the presence of Yttrium. While tanδ exhibited a declining tendency with increasing frequency and was stable at higher frequencies (20 kHz and above are capable for MLCCs devices application), capacitance exhibited a significant decrease with a sudden drop in the low-frequency range, up to 20 kHz, and then this value persisted steadily at higher frequencies.

Declarations

Author contribution statement

Suravi Islam: Conceived and designed the experiments; Analyzed and interpreted the data; Wrote the original manuscript. Nazia Khatun: Performed the experiments; Contributed reagents, materials, analysis tools or data. Md. Shehan Habib: Analyzed and interpreted the data; Wrote the paper. Syed Farid Uddin Farhad: Analyzed and interpreted the data; Contributed reagents, materials, analysis tools or data. Nazmul Islam Tanvir, Samia Tabassum, Dipa Islam, Ayesha Siddika: Performed the experiments. Md. Aftab Ali Shaikh, Ayesha Siddika, Md. Sajjad Hossain: Analyzed and interpreted the data.

Funding statement

This work was supported by Bangladesh Council of Scientific and Industrial Research (BCSIR).

Data availability statement

Data included in article/supplementary material/referenced in article.

Declaration of interest statement

The authors declare no conflict of interest.

Additional information

No additional information is available for this paper.

References

[1] A. Kareiva, S. Tautkus, R. Rapalaviciute, Sol-gel synthesis and characterization of barium titanate powders, J. Mater. Sci. 34 (1999) 4853–4857.
[2] S. Islam, S.A. Satter, N. Khatun, M.S. Hossain, S.F.U. Farhad, P. Bala, S. Tabassum, A. Siddika, Investigation of structural , dielectric and electrical properties of barium titanate ceramics Co-doped with bismuth and yttrium, J. Mol. Eng. Mater. (2019) 1–9.

[3] Y. Slimani, A. Selmi, E. Hannachi, M.A. Almessiere, G. Alfalah, L.F. Alousi, G. Yasin, M. Iqbal, Study on the addition of SiO 2 nanowires to BaTiO 3 : structure , morphology , electrical and dielectric properties, J. Phys. Chem. Solid. 156 (2021).

[4] M. Adamczyk-habrajska, Dielectric and electric properties of Ba0.996La0.004Ti0.999O3 ceramics doped with europium and hafnium ions, Materials 15 (413) (2022).

[5] S. Islam, A. Siddika, N.A. Ahmed, N. Khatun, S.N. Rahman, Synthesis and characterization of bismuth doped barium titanate, Am. Int. J. Res. Sci. Tech. Eng. Math. (AIJRSTEM) 1 (13) (2016) 28–32. http://iasir.net/aijrstemissue/aijrstemissue13-1.html.

[6] S. Islam, A. Siddika, N. Khatun, M.S. Hossain, M.H.A Begum, N.A. Ahmed, Structural, dielectric and electric properties of manganese-doped barium titanate, Int. J. Nanoelectron. Mater. 11 (4) (2018) 419–426.

[7] H. Hayashi and T. Ebina, "Effect of Hydrothermal Temperature on the Tetragonality of BaTiO3 Nanoparticles and In-Situ Raman Spectroscopy under Tetragonal–Cubic Transformation," 2018214–2018220.

[8] M. Hasan, A.K.M.A. Hossain, Computational Condensed Matter Structural , electronic and optical properties of strontium and nickel co-doped BaTiO 3 : a DFT based study, Comput. Condens. Matter 28 (2021) e00578.

[9] E.H.M.I. Sayyed, K.A. Mahmoud, Y.S.S. Akhtar, B. Albarzan, Impact of tin oxide on the structural features and radiation shielding response of some - ABO 3 perovskites ceramics (A = Ca , Sr , Ba ; B = Ti), Appl. Phys. A 127 (12) (2021) 1–12.

[10] T. Badapanda, S. Sarangi, B. Behera, S. Anwar, T.P. Sinha, R. Ranjan, E. Longo, L.S. Cavalcante, Structural Refinement , Optical and Electrical Properties, 2014, pp. 3427–3439.

[11] P. Taylor, Y. Li, Y. Hao, X. Wang, X. Yao, Studies of dielectric properties of rare earth (Y, Gd, Yb) doped barium titanate sintered in pure nitrogen, Ferroelectrics 407 (2010) 134–139.

[12] J. Qi, L. Li, Y. Wang, Y. Fan, Z. Gui, Yttrium doping behavior in BaTiO3 ceramics at different sintered temperature, Mater. Chem. Phys. 82 (2003) 423–427.

[13] J. Liu, G. Jin, Y. Chen, W. Xue, Properties of yttrium-doped barium titanate ceramics with positive temperature coefficient of resistivity and a novel method to evaluate the depletion layer width, Ceram. Int. 45 (5) (2019) 6119–6124.

[14] K. Park, C. Kim, Y. Yoon, S. Song, Y. Kim, K. Hur, Doping behaviors of dysprosium , yttrium and holmium in BaTiO 3 ceramics, J. Eur. Ceram. Soc. 29 (2009) 1735–1741.

[15] A. Alshoaibi, M.B. Kanoun, B.U. Haq, S. Alfaify, S. Goumri-said, Insights into the Impact of Yttrium Doping at the Ba and Ti Sites of BaTiO 3 on the Electronic Structures and Optical Properties, A First- Principles Study, 2020.

[16] C. Kim, K. Park, Y. Yoon, M. Hong, J. Hong, K. Hur, Role of yttrium and magnesium in the formation of core-shell structure of BaTiO 3 grains in MLCC, J. Eur. Ceram. Soc. 28 (2008) 1213–1219.

[17] J. Zhi, A. Chen, Y. Zhi, P.M. Vilarinho, L. Baptista, Incorporation of yttrium in barium titanate ceramics, Commun. Am. Ceram. Soc. 48 (1999) 8–11.

[18] P. Ren, Q. Wang, X. Wang, L. Wang, J. Wang, H. Fan, Effects of doping sites on electrical properties of yttrium doped BaTiO 3, Mater. Lett. 174 (2016) 197–200.

[19] W. Li, J. Hao, W. Bai, Z. Xu, R. Chu, J. Zhai, Enhancement of the temperature stabilities in yttrium doped, J. Alloys Compd. 531 (2012) 46–49.

[20] P.K. Patel, K.L. Yadav, Effect of yttrium on microstructure , dielectric , ferroelectric and optical, Phys. B Phys. Condens. Matter 442 (2014) 39–43.

[21] S.G. Dahotre, L.N. Singh, Synthesis and Characterization of Nanoferrite 3, 2013, pp. 199–204.

[22] Y.S.A. Selmi, E.H.M.A. Almessiere, A.B.I. Ercan, Impact of ZnO addition on structural , morphological , optical , dielectric and electrical performances of - BaTiO 3 ceramics, J. Mater. Sci. Mater. Electron. 30 (10) (2019) 9520–9530.

[23] M. Selvaraj, V. Venkatachalapathy, J. Mayandi, S. Karazhanov, J.M. Pearce, M. Selvaraj, V. Venkatachalapathy, J. Mayandi, Preparation of Meta-Stable Phases of Barium Titanate by Sol-Hydrothermal Method Preparation of Meta-Stable Phases of Barium Titanate by Sol-Hydrothermal Method, 2015, p. 117119.

[24] M. Reda and M. M. Arman, "Improvement of ferroelectric properties via Zr doping in barium titanate nanoparticles," J. Mater. Sci. Mater. Electron., vol. 1, 2022.

[25] G.K. Williamson, W.H. Hall, Discussion of the theories of line broadening, Acta Metall. 1 (1953). http://www.xray.cz/xray/csca/kol2011/kurs/dalsi-cteni/clanky/Williamson-ActaMet-1953-1-22-WH-Plot.pdf.

[26] E. Hannachi, M.A. Almessiere, Y. Slimani, R.B. Alshamrani, G. Yasin, F. Ben Azzouz, Preparation and characterization of high-T c (YBa 2 Cu 3 O 7- δ) 1-x/(CNTs) x superconductors with highly boosted superconducting performances, Ceram. Int. (2020).

[27] A. Nfissi, Y. Ababou, M. Belhajji, S. Sayouri, and T. Lamcharfi, "Structural and dielectric properties of sol–gel processed Ce-doped BaTi0.97Y0.03O3 ceramics," J. Adv. Dielectr., vol. 11, no. 1, p. 2150003.

[28] A. Kaiyum, M.A. Hossain, A.A. Momin, R. Rashid, F. Alam, M.A. Hakim, M.N.I. Khan, Structural, dielectric and magnetic properties of xNi0.50Zn0.40Mn0.10Fe2O4 + (1-x)Bi0.90La0.10Fe0.93Eu0.07O3 multiferroic composites, Mater. Res. Express 8 (2021).

[29] M.H.A. Mhareb, Y. Slimani, Y.S. Alajerami, M.I. Sayyed, E. Lacomme, A. Almessiere, P.O. Box, S. Arabia, A. Scientific, S. Arabia, S. Faculty, A. Medical, S. Faculty, M. Consultations, S. Arabia, Structural and Radiation Shielding Properties of BaTiO3 Ceramic with Different Concentrations of Bismuth and Ytterbium 3, 1982.

[30] J. Pablo, H. Lara, M. Pérez, F. Raúl, B. Hernández, J. Antonio, Structural Evolution and Electrical Properties of BaTiO 3 Doped with Gd 3 +, 2017.

[31] J. Suchanicz, A. Sternberg, Influence of Compressive Stress on Dielectric and, 2013, p. 4.

[32] L.H. Robins, D.L. Kaiser, L.D. Rotter, L.H. Robins, D.L. Kaiser, L.D. Rotter, P.K. Schenck, D. Rytz, Investigation of the structure of barium titanate thin films by Raman spectroscopy, J. Appl. Phys. 7487 (2017).

[33] P. Sá, I. Bdikin, B. Almeida, A.G. Rolo, D. Isakov, Ferroelectrics Production and PFM Characterization of Barium Titanate Nanofibers Production and PFM Characterization of Barium, Taylor Fr., 2012, pp. 48–55.

[34] Y. Zhang, J. Hao, C.L. Mak, X. Wei, Effects of site substitutions and concentration on upconversion luminescence of Er 3 + -doped perovskite titanate, Opt. Publ. Gr. 19 (3) (2011) 179–184.

[35] S.N. Rahman, N. Khatun, S. Islam, N.A. Ahmed, Int. J. Emerg. Technol. Computational and applied sciences (IJETCAS) comparative studies of cerium and zirconium doped barium titanate, Int. Assoc. Sci. Innov. Res. (2014) 15–19.

[36] P. Blanchart, J.F. Baumard, P. Abelard, Effects of yttrium doping on the grain and grain-boundary resistivities of BaTiO3 for positive temperature coefficient thermistors, J. Am. Ceram. Soc. 75 (5) (May 1992) 1068–1072.

[37] S. More, R. Dhokne, S. Moharil, Dielectric relaxation and electric modulus of polyvinyl alcohol – zinc oxide composite films, Mater. Res. Express 4 (2017).

[38] T. Badapanda, C.V.R.G. Univeristy, S.K. Rout, S. Panigrahi, T.P. Sinha, Dielectric behavior of yttrium doped barium-zirconium-titanate ceramics dielectric behavior of yttrium doped barium-zirconium-titanate ceramics, J. Kor. Phys. Soc. 55 (2009) 749–753.

[39] J. Tauc, R. Grigorovici, A. Vancu, Optical Properties and Electronic Structure of Amorphous Germanium 627, 1966, pp. 627–637.

[40] B.C. Ghos, S.F.U. Farhad, M.A.M. Patwary, S. Majumder, M.A. Hossain, N.I. Tanvir, M.A. Rahman, T. Tanaka, Q. Guo, Influence of the substrate, process conditions, and postannealing temperature on the properties of ZnO thin films grown by the successive ionic layer adsorption and reaction method method, ACS Omega 6 (2021) 2665–2674.

[41] K. Suzuki, K. Kijima, Optical Band Gap of Barium Titanate Nanoparticles Prepared by RF-Plasma Chemical Vapor Deposition Optical Band Gap of Barium Titanate Nanoparticles Prepared by RF-Plasma Chemical Vapor Deposition, 2014, pp. 2081–2083.

[42] R. Kale, C. Lokhande, Influence of air annealing on the structural, optical and electrical properties of chemically deposited CdSe nano-crystallites, Appl. Surf. Sci. 223 (4) (Feb. 2004) 343–351.